AAS 14-467

VARIOUS TRANSFER OPTIONS FROM EARTH INTO DISTANT RETROGRADE ORBITS IN THE VICINITY OF THE MOON

Lucía Capdevila*, Davide Guzzetti* and Kathleen C. Howell†

Future applications within the Earth-Moon neighborhood, under a variety of mission scenarios, such as NASAs Asteroid Redirect Robotic Mission (ARRM), may exploit lunar Distant Retrograde Orbits (DROs). Thus, further investigation of transfers to and from these orbits is useful. The current study is focused on transfer trajectory options that employ impulsive maneuvers to deliver a vehicle from Low Earth Orbit (LEO) into various lunar DROs. The stability region surrounding specific DROs, as modeled in the Earth-Moon Circular Restricted Three-Body Problem (CR3BP), may also serve to facilitate the transfer design process and is explored within that context. Representative solutions are transitioned to an ephemeris model and station keeping costs are compared.

INTRODUCTION

The recently proposed concept for NASA's Asteroid Redirect Robotic Mission (ARRM) is based upon the capture of an asteroid and the relocation of the object into the vicinity of the Moon; one initial option under this proposal, in fact, is the insertion of the asteroid into a lunar Distant Retrograde Orbit (DRO).[1] Subsequent manned missions might then be expected to deliver a crew to the asteroid for exploration and investigation.[2] The asteroid redirect concept is not the sole purpose for further analysis of DROs and transfer strategies from the Earth to reach these orbits, however. Future applications within the Earth-Moon neighborhood, under a variety of mission scenarios, may exploit such DROs. Thus, further general investigations of transfers to and from these orbits are useful.

Distant retrograde orbits are well-known trajectory types.[3,4,5,6,7] Such orbits have also been the focus of a number of investigations concerning transfers. However, most of these transfers have involved DROs about the Earth or Jupiter's moon Europa.[8,9,10,11,12] With the exception of two transfer trajectories from Earth into a lunar DRO, as investigated by Ming and Shijie in 2009,[13] and a transfer from LEO into a three-dimensional lunar DRO, as constructed by Vaquero in 2012,[14,15] few transfers into lunar DROs are available in the literature. The current analysis is focused on transfer trajectory options that employ impulsive maneuvers to deliver a vehicle from Low Earth Orbit (LEO) into various lunar DROs. The stability region surrounding specific DROs, as modeled in the Earth-Moon CR3BP, may also serve to facilitate the transfer design process and is explored within that context. Thus, this analysis may be useful in the development of future trajectory design strategies for both manned and robotic missions involving lunar DROs.

CIRCULAR RESTRICTED THREE BODY PROBLEM

In this investigation, the motion of the spacecraft in the Earth-Moon environment is modeled in terms of the CR3BP. The CR3BP equations of motion (EOMs) can be expressed as follows

$$\ddot{x} - 2\dot{y} = \frac{\partial U}{\partial x}, \ddot{y} + 2\dot{x} = \frac{\partial U}{\partial y}, \ddot{z} = \frac{\partial U}{\partial z} \tag{1}$$

*Ph.D. Student, School of Aeronautics and Astronautics, Purdue University, 701 W. Stadium Ave., West Lafayette, IN, 47907-2045.
†Hsu Lo Distinguished Professor of Aeronautics and Astronautics, School of Aeronautics and Astronautics, Purdue University, 701 W. Stadium Ave., West Lafayette, IN, 47907-2045.

where U is the pseudo-potential function. These equations describe the position of the spacecraft, $\vec{R} = [x, y, z]^T$, and its velocity, $\vec{V} = \dot{\vec{R}} = [\dot{x}, \dot{y}, \dot{z}]^T$, in terms of components in the rotating reference frame. The rotating reference frame is centered at the barycenter of the Earth-Moon system, B, and rotates with the primaries. The rotating $\hat{x}$ axis is directed from the Earth to the Moon, $\hat{y}$ is perpendicular to $\hat{x}$ and in the plane of the primaries, and $\hat{z} = \hat{x} \times \hat{y}$ completes the right handed triad. The rotating reference frame is related to the inertial frame through a simple rotation, θ, about the $\hat{z} = \hat{Z}$ axis.

The rotating frame coordinates are nondimensional based on the characteristic length, $L^* \cong 384{,}388$ km (the distance between the Earth and the Moon), and time, $T^* = \sqrt{\frac{L^{*3}}{G(m_{\text{Earth}}+m_{\text{Moon}})}}$, where G is the universal gravitational constant. The pseudo-potential is denoted as U in equations (1), and is computed as $U = \frac{1}{2}\left(x^2+y^2\right) + \frac{(1-\mu)}{r_{13}} + \frac{\mu}{r_{23}}$, where the characteristic mass parameter, μ, is a function of the masses of the Earth, m_{Earth}, and the Moon, m_{Moon}, such that $\mu = \frac{m_{\text{Moon}}}{m_{\text{Earth}}+m_{\text{Moon}}}$. For this investigation $\mu = 0.012151$. The scalar quantities in the denominator, r_{13} and r_{23}, are the distances to the spacecraft measured from the Earth and the Moon, respectively. The CR3BP EOMs admit an integral of the motion, that is, the Jacobi constant, C. This constant is a function of the pseudo-potential and the speed such that $C = 2U - \left(\dot{x}^2+\dot{y}^2+\dot{z}^2\right)$. The Jacobi constant proves useful in distinguishing regimes of motion in the CR3BP.[16]

DISTANT RETROGRADE ORBITS

The emergence of DROs in the literature is not recent. As early as 1968, Broucke's work offers evidence of the existence of DROs in the Earth-Moon system. Broucke's comprehensive investigation on x-axis symmetric periodic orbits in the planar Earth-Moon CR3BP mentions a family of retrograde lunar orbits labeled family "C". Members with single loops around the Moon, as viewed in the rotating reference frame, are observed as stable. Broucke also notes that family C corresponds to Stromgren's class "f".[17] Several authors have since contributed to the understanding of the dynamical properties of DROs and the surrounding neighborhood in different systems.[3,4,6,7] In Hill's limiting case of the planar restricted three-body problem, these orbits were investigated by Hénon. The 1969 publication by Hénon refers to these orbits as family "f".[3] For illustration, the family in the Earth-Moon CR3BP is plotted over a large range in Figure 1(a). The color of each orbit indicates the Jacobi constant value, specified by the colorbar on the right. It is apparent that the path of some members extends very far from the Moon, hence the name Distant Retrograde Orbits (DROs). It is also evident that DROs orbiting close to the Moon possess high Jacobi constant values, close to the Jacobi constant values for L_1 ($C_{L_1} = 3.18834$) and L_2 ($C_{L_2} = 3.17216$), while DROs with close passes of the Earth are characterized by much lower Jacobi constant values.

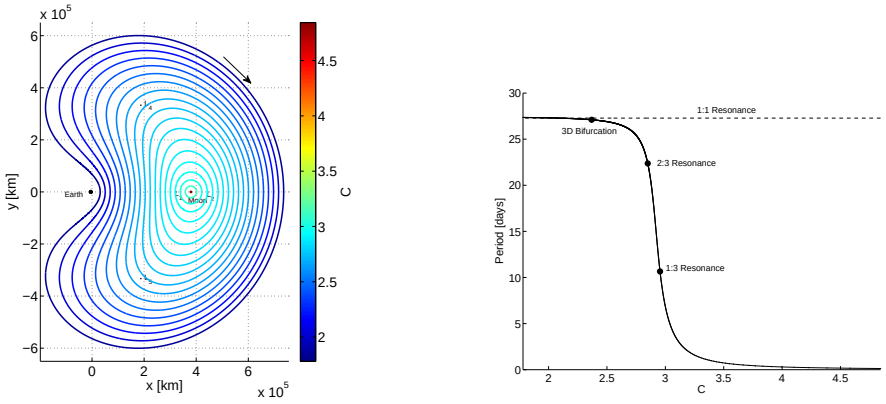

(a) Geometry and Jacobi constant

(b) Orbital period

Figure 1. DRO properties in the Earth-Moon CR3B problem

The period of an orbit complements the geometry in terms of the speed of the spacecraft along a particular path in comparison to others; speed is also indicative of the specific three-body system. The DRO orbital periods in Figure 1(b), are plotted as a function of Jacobi constant. DROs close to the Moon (high C) are characterized by very short periods, but DROs grow in size (decreasing C) as the orbital period passes through the 1:3 and 2:3 lunar resonances, and asymptotically approaches a 1:1 resonance with the Moon. From Broucke's 1968 report, a family of Earth retrograde orbits also exists in the Earth-Moon planar CR3BP, i.e., family "A_1". As Earth DROs evolve from orbits in the close vicinity of the Earth to orbits with close passages of the Moon, they appear as a mirror image of the lunar DROs across the line $x \approx 0.5$. Similar to the family of lunar DROs, as Earth DROs approach the collision orbit with the Moon, the period of these orbits approaches the period of the primary system. Also, notable is the fact that not all Earth DROs are stable.[17]

The stability of a periodic orbit reveals much information concerning the behavior of the associated neighboring flow, and a change in stability can signal bifurcations with other families of periodic orbits. As previously mentioned, lunar DROs are stable when only planar motion is considered. Nonetheless, several period-multiplying bifurcations can be detected. The lowest multiplicity occurs at $C \cong 2.95494$ and $C \cong 2.84913$, where a period-tripling bifurcation occurs. Hénon labeled this family as "g3".[4] Thus, such three-revolution periodic orbits are denoted as period-3 DROs (P3DROs). Higher multiplicity period-multiplying bifurcations also exist, as introduced by Markellos in 1974 in the Sun-Jupiter CR3BP, and in 2007 by Douskos, Kalantonis and Markellos in the Earth-Moon system.[5,7] However, when out-of-plane motion is considered, a bifurcation with a three-dimensional family is detected at $C \cong 2.36871 < C_{L_2} < C_{L_1}$ as noted by Vaquero and Howell. The three-dimensional family of orbits is stable, while DROs that exist at $C > 2.36871$ are unstable.[14,15]

Although P3DROs are only one of numerous period-multiplying families that bifurcate from the planar DRO family, they play an important role in characterizing the neighboring DRO dynamics. Given that a DRO at a particular energy level exists, a corresponding P3DRO also exists. Some characteristics of both, P3DRO and DRO families, at select energy levels, appear in Figure 2. For the sample trajectories, it is evident that the path along the P3DRO remains loosely in the vicinity of the DRO. The time along one revolution across the family of P3DROs evolves similarly to the DRO orbital period, as demonstrated in Figure 2(d). However, in contrast with DROs, P3DROs are linearly unstable. As unstable orbits, P3DROs have associated stable and unstable manifolds, that is, flow that asymptotically approaches or departs the orbit, respectively. Stable DROs, however, only possess an associated center manifold, that is, flow that neither departs or approaches the orbit. This 'DRO stability region' is comprised of the various period-multiplying families previously mentioned as well as quasi-periodic DROs (QPDROs).[7] In fact, the P3DRO stable and unstable manifolds bound the DRO stability region at all energy levels.[11] However, the stability region is destroyed at the each of the period-tripling bifurcations previously highlighted. This phenomenon was first observed by Hénon in Hill's problem; Markellos, then, confirmed it in the Sun-Jupiter CR3B problem.[4,5] Winter, in 2000, and then Douskos, Kalantonis and Markellos, in 2007, corroborated the same dynamical behavior in the Earth-Moon CR3BP.[6,7]

The DRO stability region proves useful to transition results from the CR3BP into the ephemeris model. To better understand and visualize this region, consider the energy level $C = 2.91$. The lunar DRO that exists at this Jacobi constant value is plotted in black in Figure 3(a). The green path is the P3DRO, and a QPDRO at the same energy level appears in gray. However, there exists an infinity of QPDROs at this same energy level, but, due to the high number of lunar revolutions, it is not useful to visualize them in the $x - y$ space. Instead, the dynamical structures in the region surrounding the DRO are more easily visualized on a surface of section. Consider a two-sided surface of section along the x-axis at a specific Jacobi constant value, C^*, $y = 0, C = C^*$. The surface associated with $C^* = 2.91$ yields the map that appears in Figure 3(b). It is apparent that similar structures emerge for positive (left) and negative (right) y-velocities, that is, on both DRO crossings of the x-axis. Focusing only on the left half with $\dot{y} > 0$, the DRO is represented as a single black dot, several QPDROs appear in gray, and the P3DRO appears as three hyperbolic points on the section. As previously mentioned, the stable (blue) and unstable (red) P3DRO manifolds bound the stability region. Furthermore, the distance between the DRO fixed point, and the P3DRO hyperbolic point that lies on the x-axis can be used to represent the width of the stability region. If these fixed points are computed at different energy levels, it is possible to generate a graphical representation that indicates the width of the

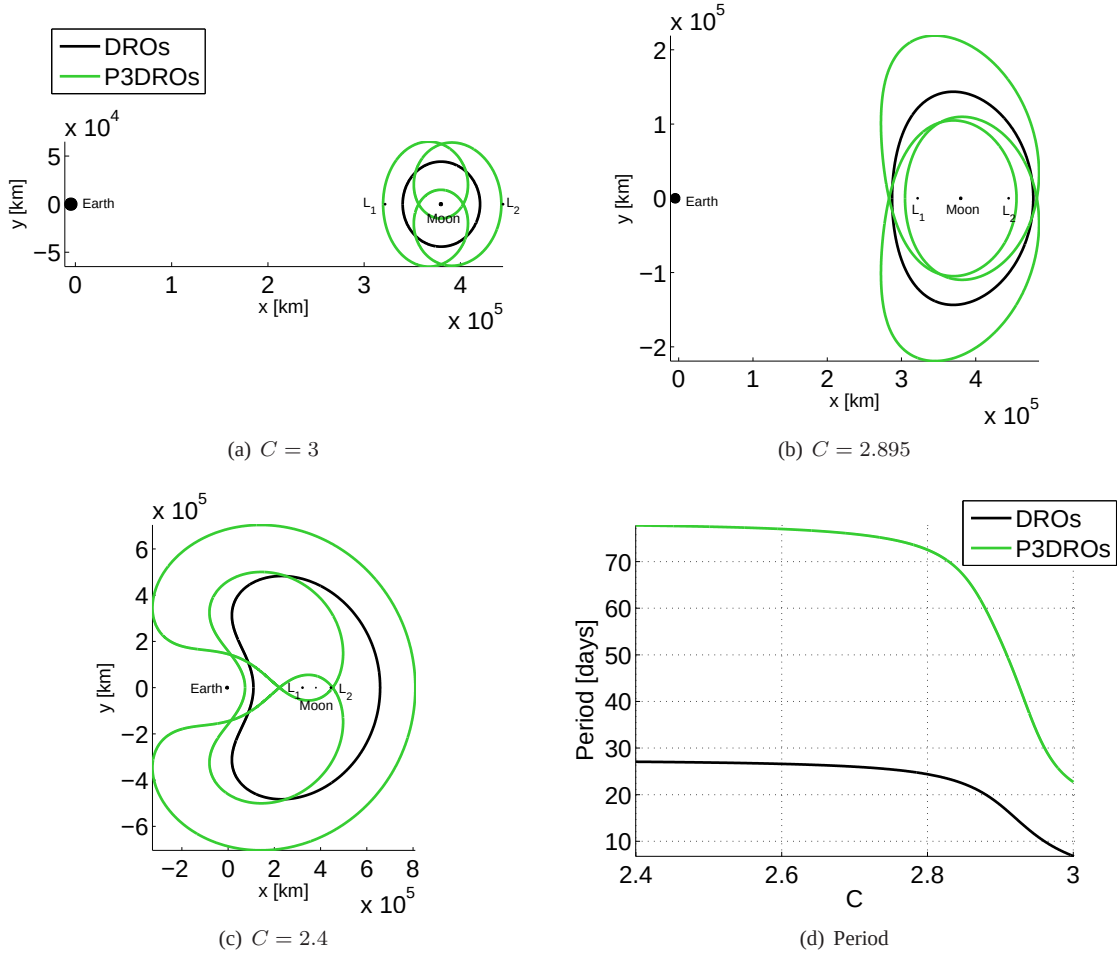

(a) $C = 3$ (b) $C = 2.895$

(c) $C = 2.4$ (d) Period

Figure 2. P3DRO properties in the Earth-Moon CR3BP

stability region at different Jacobi constant values. A limited range of information is plotted in Figure 3(c) across the DRO, period-3 and period-4 DRO families in the (x_0, C) plane. In the figure, x_0 is the x-position of the periodic orbit as it crosses the x-axis perpendicularly ($\dot{x} = 0$) with positive y-velocity ($\dot{y} > 0$), and C is the orbit's Jacobi constant. As expected, DROs and P3DROs intersect when $C \cong 2.95494$ and $C \cong 2.84913$ at the period-tripling bifurcations. The quasi-periodic region surrounding the DRO disappears at these Jacobi constant values. The period-4 DROs originate from a period-quadrupling bifurcation with the DRO family, at $C \approx 2.99572$, and exist within the stability region.[7]

RESULTS

To explore the solution space and the dynamical behavior from the perspective of the three-body problem, analysis is initially focused on the planar problem. Thus, some transfer arcs from a 200-km altitude orbit about the Earth to various DROs and the surrounding stability region are first investigated. A scheme to design transfers into the DRO stability region and then into a DRO is described, and sample results are provided. Representative results are transitioned to an ephemeris model. To investigate the impact of non-periodic and out-of-plane perturbations, stationkeeping costs are also sampled.

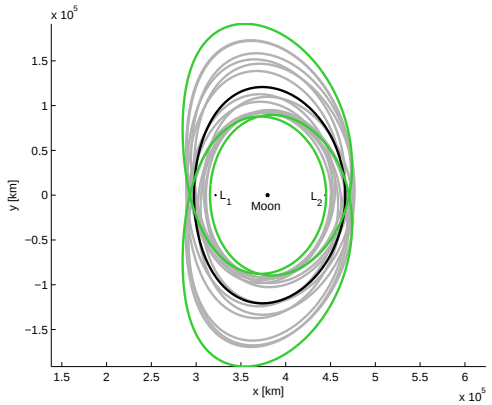

(a) DRO, Period-3 DRO and QPDRO at $C = 2.91$

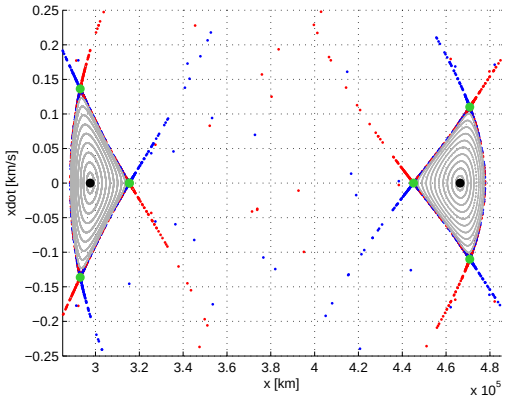

(b) DRO Stability Region at $C = 2.91$

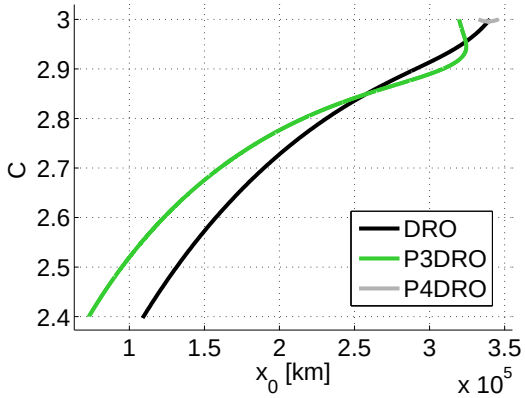

(c) Size of DRO stability region at various Jacobi constant values

Figure 3. DRO Stability Region

Differential Corrections

To construct a transfer arc in the restricted problem, a corrections process is simple and efficient to implement. Using a suitable initial guess and a multi-dimensional Newton-Raphson differential corrections scheme, it is possible to numerically determine a trajectory that departs a circular Earth orbit tangentially, and arrives at an x-position and velocity that matches the connecting trajectory.

The differential corrections process allows adjustment of certain variables to meet a set of specified constraints. The algorithm constrains departure from a circular Earth orbit, and the initial transfer velocity is required to be tangential to the Earth orbit. Upon arrival, the final x-position and velocity along the transfer path are required to match that of the destination trajectory at the crossing of the x-axis ($y = 0$). To accomplish these requirements, the initial position along the Earth circular orbit, the initial velocity along the transfer trajectory, and the transfer time are allowed to vary.

Direct Transfers to Lunar DRO via L_1 Lyapunov Orbits: Lunar Near-Side Insertion

In the absence of manifold structures associated with a stable destination orbit, a Hohmann transfer is commonly employed as an approximation for the computation of a transfer trajectory from the vicinity of a gravitating body to a stable orbit in the CR3BP. Thus, understanding the geometry, ΔV cost and the Time of Flight (TOF) associated with Hohmann transfers computed in the Two-Body Problem (2BP) is insightful as

a baseline for comparison with transfers constructed in the CR3BP.

The geometry of the Hohmann transfers can appear very different depending on the reference frame used for visualizing the trajectory. Figure 4(a) demonstrates three Hohmann transfers as viewed in the inertial Earth-centered frame, where light blue, gray and pink dashed lines indicate the radius distance to L_1, the Moon, and L_2, respectively. Each of the three transfers originate from a 200-km altitude circular Earth orbit, and arrive at a circular orbit with radius corresponding to the locations of L_1, the Moon, and L_2, respectively. When viewed in the barycentered rotating reference frame, the inertial ellipses appear as plotted in Figure 4(b). The ΔV cost for an Earth LEO departure and the TOF are summarized for each transfer in Table 1. In

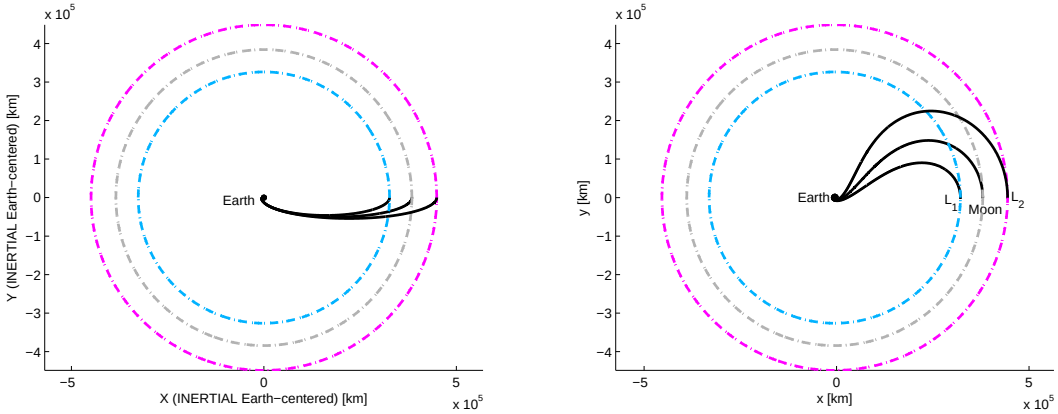

(a) Inertial, Earth-centered view

(b) Rotating, barycentered view

Figure 4. Hohmann Transfers to L_1, the Moon, and L_2 in the 2BP

Table 1. Hohmann Transfers to L_1, the Moon, and L_2 in the 2BP

Destination Location	L_1	**Moon**	L_2
ΔV_1 [km/s]	3.1178	3.134	3.1473
TOF [days]	3.9117	4.9775	6.2591

this investigation, more accurate transfers are then computed using the differential corrections process as an initial investigation of transfers from the vicinity of the Earth into stable lunar DROs in the CR3BP.

Distant retrograde orbits, however, are only one type of family in the lunar region – even in the planar problem. Numerous other families of periodic orbits exist, and are available in the literature. One such family is the set of periodic Lyapunov orbits. Parts of the family of DROs and the L_1 Lyapunov orbits appear together in Figure 5(a). The color of each orbit indicates the associated Jacobi constant value, C. These two planar families of periodic orbits overlap in geometry, but they occupy very different locations in the energy space. Lyapunov orbits about L_1 exist at a higher energy level than DROs. However, the size of the energy gap between the two families decreases as the orbits extend beyond the vicinity of the Moon. A similar phenomenon occurs in comparisons of L_2 Lyapunov orbits and lunar DROs. For some DROs, it is possible to locate an adjacent L_1 Lyapunov orbit, such that these orbits share a crossing of the x-axis, in position, when $\dot{y} > 0$. For example, the DRO that exists at $C = 2.91$ and the adjacent L_1 Lyapunov appear as viewed in the rotating, barycentered reference frame in Figure 5(b), where the symbols "o" and "$*$" indicate the initial and final state along each orbit, respectively. When these orbits are viewed in the Earth-centered, inertial reference frame, they appear as in Figure 5(c). Similarly, the Moon-centered, inertial view of both orbits are plotted in Figure 5(d). Note that, while these orbits are periodic in the rotating frame, they are not periodic in the inertial frame. Evident from the non-elliptical geometry of the DRO and Lyapunov orbit

paths in either the Earth- or Moon-centered inertial frames, the gravitational influence of the third body is significant. Furthermore, the adjacent L_1 Lyapunov orbit associated with a lunar DRO can be employed to re-direct an inbound Earth transfer to arrive at the DRO on the near side of the Moon.

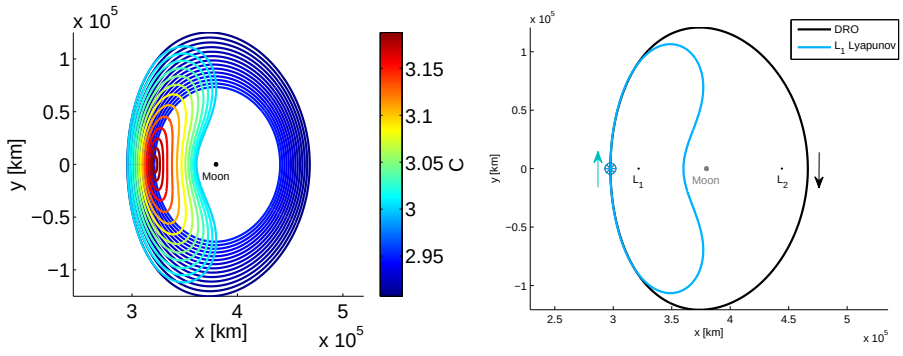

(a) Geometry of DROs and adjacent L_1 Lyapunov orbits, and Jacobi constant, C

(b) DRO at $C = 2.91$ and adjacent L_1 Lyapunov in rotating, barycentered view

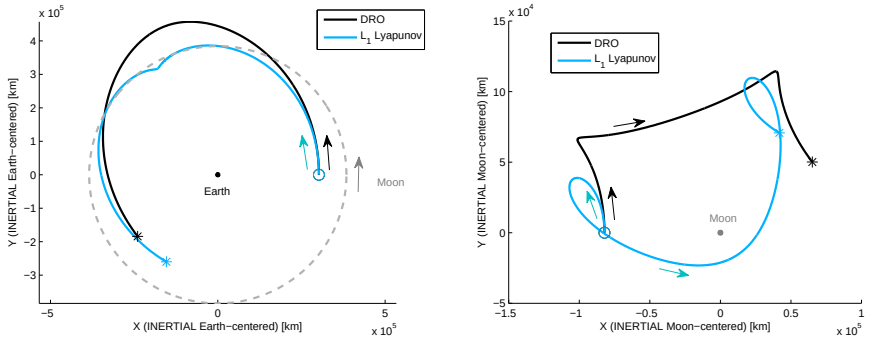

(c) DRO at $C = 2.91$ and adjacent L_1 Lyapunov in inertial, Earth-centered view

(d) DRO at $C = 2.91$ and adjacent L_1 Lyapunov in inertial, Moon-centered view

Figure 5. DRO and adjacent L_1 Lyapunov orbit comparison

Given a destination DRO, it is possible to deliver a transfer trajectory with a DRO insertion on the near-side of the Moon via corresponding adjacent L_1 Lyapunov. After departure from LEO, these transfers incorporate an insertion maneuver to shift into an L_1 Lyapunov, where $y = 0$ and $\dot{y} < 0$ in the rotating frame. The spacecraft, then, follows the Lyapunov path for exactly half a period. When the L_1 Lyapunov and DRO coincide in position, a final maneuver is implemented to insert into the DRO. Since the DROs in this investigation are completely in the plane of the primaries, they are uniquely identified by their maximum excursion in the y-direction, that is, their y-amplitude as measured from the x-axis. Let this quantity be denoted as A_y. As A_y increases, the farther the excursion of the DRO path relative to the Moon. For each A_y amplitude, the transfer from LEO includes an associated departure maneuver, ΔV_1, an L_1 Lyapunov insertion maneuver, ΔV_2, and ΔV_3 for DRO insertion. The geometry for such transfers in the xy plane as viewed in the rotating reference frame is represented in Figure 6(a), where each transfer path is colored consistent with the total ΔV cost, and the colorbar on the right translates color into ΔV values in km/s. The time to reach the L_1 Lyapunov orbit, T_1, and the additional time until arrival onto the DRO, T_2, also vary as a function of the DRO amplitude A_y.

A trajectory path that links a LEO to the L_1 Lyapunov orbit, is essentially a high energy arc, comparable to an outbound Hohmann transfer arc in the 2BP. The LEO departure cost for transfers with lunar near-side DRO insertions range between $3.1165 \leq \Delta V_1 \leq 3.1317$ km/s, and the TOF to the L_1 Lyapunov orbit insertion point is within the range $4.15 \leq T_1 \leq 5.67$ days. Higher LEO departure costs and TOFs correspond to larger amplitude A_y DROs. Therefore, both of these ranges are comparable to the ΔV_1 and TOF ranges that

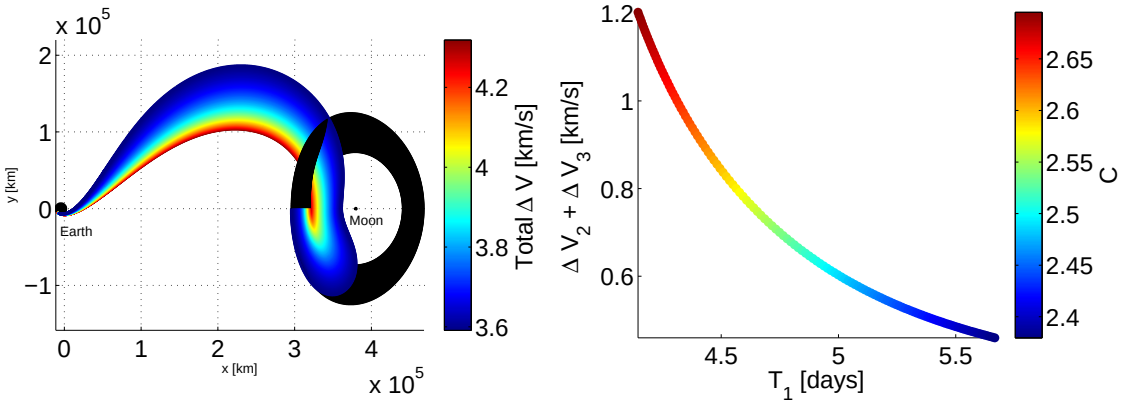

(a) Geometry and total ΔV

(b) L_1 Lyapunov and DRO insertion cost, T_1, and transfer Jacobi constant, C

Figure 6. Direct transfers into lunar DRO via L_1 Lyapunov Orbits

exist between standard Hohmann transfers to the L_1 location, and to the Moon's location as listed in Table 1. Many authors have investigated direct transfers into lunar L_1 orbits from Earth.[18,19] One of the more recent studies by Folta et al. computes direct transfers from a 200-km altitude LEO into L_1 Lyapunovs in the Earth-Moon CR3BP. For a similar L_1 Lyapunov orbit amplitude range, the insertion cost reported by Folta et al. is approximately within 350-650 m/s.[20] In this investigation, ΔV_2 decreases monotonically from 710.34 m/s, corresponding to the smallest L_1 Lyapunov that appears in Figure 6(a), to 368.61 m/s for the largest orbit in the figure. Therefore, the L_1 Lyapunov insertion cost in this investigation is in agreement with previous results.

The transfers to the lunar near-side of the DRO also includes a second leg, i.e., of a half-revolution along an L_1 Lyapunov orbit. In comparison to the inbound transfer arc from Earth, L_1 Lyapunov orbits are slower dynamical structures. Therefore, it is not surprising that time along the second leg is nearly as long as the first arc. The time spent along the Lyapunov orbit ranges from 5.84 to 9.40 days, as orbits grow in size. Upon arrival at the DRO, a final maneuver is required to bridge the gap in energy existing between the arriving L_1 Lyapunov arc and the DRO. Recall from Figure 5(a), that the energy gap between the families decreases as orbits become larger. Thus, the magnitude of this maneuver equals 491.96 m/s, for the smallest L_1 Lyapunov and DRO in Figure 6(a), and decreases monotonically to 90.94 m/s for the largest orbit pair.

The ΔV costs and TOFs for transfers to DROs via L_1 Lyapunovs are characterized by the impact of the lunar passage. Given the relatively minor variation in the Earth departure cost, the total difference in the ΔV's is driven by the Lyapunov and DRO insertion ΔVs ($\Delta V_2 + \Delta V_3$), ranging from 1.2023 km/s to 0.4595 km/s, decreasing monotonically as the location of ΔV_2 approaches the Moon. Similarly, total TOF is overwhelmed by the L_1 Lyapunov half-period, and varies from 9.9895 to 15.0189 days, increasing with proximity to the Moon. Furthermore, given the mirror theorem, any trajectory in the CR3BP possesses a corresponding mirror image that exists across the x-axis in negative time.[21] In positive time, then, the first leg of these transfers and their mirror image form one continuous cislunar free-return trajectory similar to those by Folta et. al.[20]

Direct Transfers to Lunar DRO: Lunar Far-Side Insertion

An alternative to transfers with DRO insertion on the near-side of the Moon, transfers to the lunar far-side insert directly into the DRO. These transfers only require two maneuvers, one to depart the LEO, and one to insert into the DRO. Representative far-side arrivals appear in Figure 7(a) in the xy plane in the rotating reference frame. The colorbar on the right indicates the total ΔV associated with each color. It is apparent that the total ΔV cost decreases with increasing DRO size. The far-side transfers consist of a high energy arc that delivers the spacecraft from LEO to the DRO far-side distance, again comparable to a Hohmann

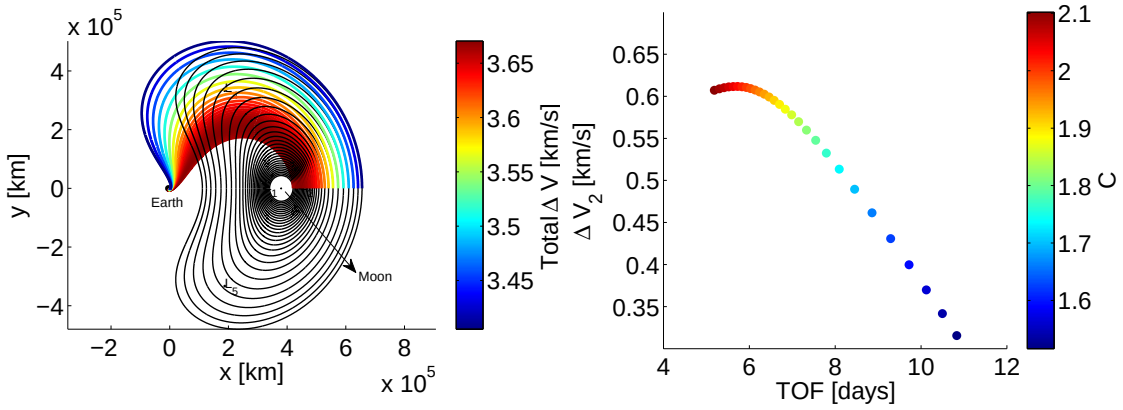

(a) Geometry and total ΔV

(b) ΔV_2, TOF, and transfer Jacobi constant, C

Figure 7. Direct transfers into lunar DRO with far-side insertion

transfer in the 2BP. For the altitude range corresponding to the DROs far-side insertions, the LEO departure cost along the Hohmann arc is in the range 3.1428 - 3.1728 km/s, where the higher cost corresponds to the highest altitude. Transfers to the far-side in the CR3BP depart the vicinity of the Earth after a maneuver with magnitude within $3.1451 \leq \Delta V_1 \leq 3.1734$ km/s, confirming the similarity with 2BP Hohmann Earth departure costs. The Hohmann transfer TOF increases from 5.77 to 11.14 days, as the destination altitude grows. Much like the Hohmann TOF, CR3BP transfers with lunar far-side insertions exhibit monotonically increasing flight times, i.e., $5.19 \leq$ TOF ≤ 10.90 days. Thus, neither the Earth departure cost, or the TOF are surprising results.

The DRO insertion cost for transfers from the vicinity of the Earth to the lunar far-side reflects the energy required to bridge the gap in Jacobi constant between the inbound transfer arc and the destination DRO. The DRO insertion cost, ΔV_2, ranges from a minimum of 310.52 m/s, for the largest orbit in Figure 7(a), to a maximum of 611.75 m/s. This maximum, however, does not occur at the smallest DRO. In fact, the maximum insertion cost occurs for a DRO whose x-axis crossings are loosely in the neighborhood of L_1 and L_2, which is, roughly, also the vicinity of the Moon's sphere of influence. Similar to transfers from Earth to L_1 orbits, transfers to orbits about L_2 have also been investigated by many authors.[18,22] A recent study by Folta et al. includes direct transfers from a 200-km altitude circular Earth orbit to L_2 Lyapunov orbits. The Lyapunov insertion maneuvers range from 650 m/s to 975 m/s.[20] Comparing the DRO insertion cost to that associated with L_2 Lyapunovs, it is apparent that L_2 Lyapunovs are more expensive in terms of insertion since L_2 Lyapunovs exist at lower energies than DROs and, therefore, exist at a further distance in the energy space from the high-energy inbound transfer arc.

Given transfers with both lunar near- and far-side DRO insertions, it is apparent that each transfer type possesses advantages and disadvantages. While transfers with DRO insertions on the lunar far-side are faster than transfers with lunar near-side insertion, transfers to the near-side require less propellant than transfers to the far-side for certain DRO amplitudes. Similar to transfers to the lunar near-side, transfers to the far-side are approximately half of a translunar free-return transfer, consistent with Folta et. al.[20]

Transfers to Lunar DRO with Close Lunar Flyby

Exploiting the Adaptive Trajectory Design (ATD) software package,[23] transfers to DROs with lunar far-side insertions can also be used in combination with a lunar conic for an initial transfer design to a DRO that incorporates a lunar flyby, similar to the transfer types explored in Muirhead, as well as Stich.[1,2] Also using ATD, the initial design can be corrected for continuity in position and velocity everywhere along the path with the exception of the expected maneuver locations: near the lunar flyby (ΔV_1), and at DRO insertion (ΔV_2). Finally, a continuation process in terms of maximum total ΔV ($= \Delta V_1 + \Delta V_2$) within the ATD

environment, yields a transfer with a significant reduction in the total maneuver ΔV. Note that the ΔV at departure from LEO is not included in the following discussion because it does not differ significantly from the values already mentioned.

For example, consider the design of a transfer with a lunar flyby to reach the DRO that exists at $C = 2.91$, with a period approximately of 16.44 days. The vehicle is delivered to the lunar vicinity along a direct transfer path with a lunar far-side insertion into the smallest DRO in Figure 7(a). A lunar conic then delivers the spacecraft to the DRO at $C = 2.91$. After this design is corrected for continuity in position and velocity, excluding the maneuver locations, the resulting transfer appears in Figure 8(a), where the maneuver locations are denoted by the red "$*$" symbol. Continuation to reduce the total ΔV yields the final design in Figure 8(b). The final design requires $T_1 = 5.08$ days to reach the lunar vicinity. Near the Moon, a $\Delta V_1 = 151.021$ m/s maneuver is executed. An additional $T_2 = 7.75$ days are required to reach the DRO insertion location, where a final maneuver of $\Delta V_2 = 68.9662$ m/s is required. The total $\Delta V = 219.9872$ m/s, and the total transfer time is 12.83 days. In comparison to the direct transfer with insertion on the lunar far-side for the same DRO, i.e., $C = 2.91$, the transfer that incorporates a lunar flyby requires 7.642 days longer to reach the destination DRO. However, including a lunar flyby reduces the total ΔV by 387.1728 m/s. Other DROs

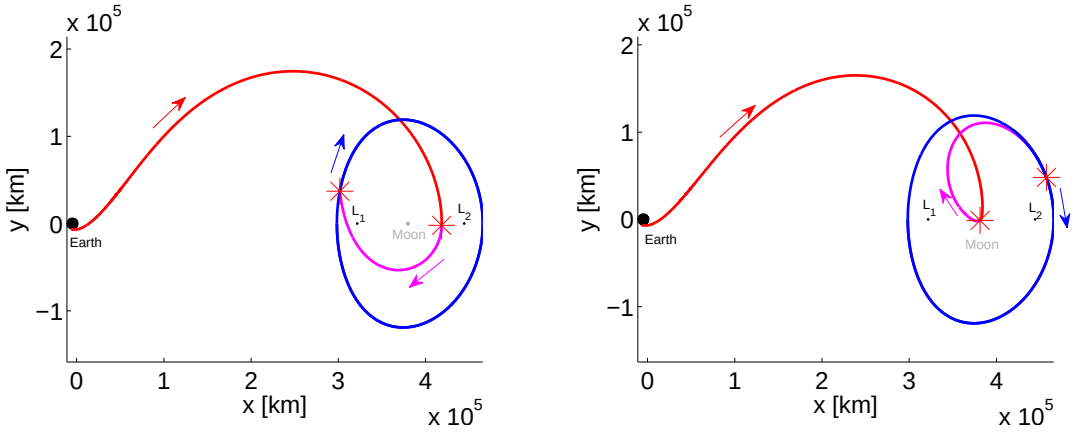

(a) Initial design corrected for position and velocity continuity

(b) Final design with reduced total ΔV

Figure 8. Transfer into lunar DRO at $C = 2.91$ with lunar flyby

are also available after a lunar encounter. Using a similar process, it is possible to design a transfer with a lunar flyby to a larger DRO, for example, one characterized by a Jacobi constant value of $C = 2.75365$ and a 25.4973-day period. The final transfer design for the larger destination DRO appears in Figure 9. This transfer delivers the spacecraft to the lunar vicinity in $T_1 = 4.14$ days. The maneuver executed near the Moon is $\Delta V_1 = 147.1516$ m/s in magnitude. After $T_2 = 17.19$ days, a $\Delta V_2 = 72.8481$ m/s DRO insertion maneuver is required. Thus, the total ΔV (219.9997 m/s) for the transfer with a lunar flyby (to a DRO with a larger A_y amplitude) is 264.2503 m/s cheaper than the transfer that delivers the spacecraft directly to the DRO on the lunar far-side, but the total transfer time (21.3294 days) is 12.83 days slower. It is apparent that close lunar flybys can reduce ΔV requirements, as expected. From a broader perspective, incorporating a lunar encounter en route to a DRO is straightforward and clearly adds opportunities to reach a variety of DRO destinations.

Direct Transfers to Lunar DRO Stability Region: Lunar Far-Side Insertion

Recall that, with the exception of two energy levels, DROs generally are surrounded by a region of stability. Similar to transfers from LEO to various periodic orbits, it is also possible to construct transfers to QPDROs by requiring that the final x-position and the velocity along the transfer arc simply locates the state within the stability region as defined by the manifolds of the unstable P3DRO at a particular energy level. For example, recall the QPDRO plotted in Figure 3(a) that exists at $C = 2.91$. The transfer to this QPDRO

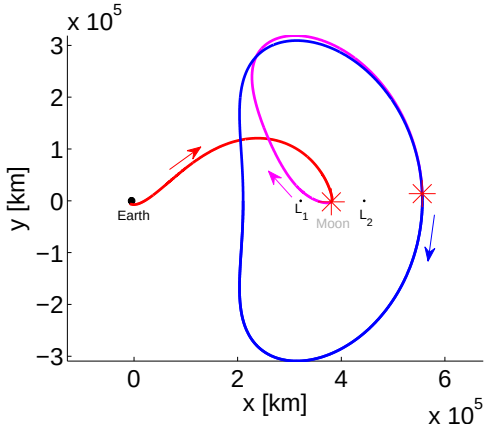

Figure 9. Transfer into 25.4973-day period lunar DRO ($C = 2.75365$)

from LEO has a departure $\Delta V_1 = 3.1503$ km/s, consistent with the departure cost associated with the 2BP Hohmann transfer to L_2 as listed in Table 1. After a transfer time of $T = 5.9849$ days, the QPDRO insertion maneuver is $\Delta V_2 = 586.5$ m/s, yielding a total ΔV of 3.7368 km/s. The transfer path is plotted in Figure 10 in dark purple, and the QPDRO is gray as viewed in the xy plane in the rotating reference frame. In comparison, the transfer directly to the DRO at this energy level requires a slightly higher insertion maneuver, $\Delta V_2 = 602.0297$ m/s, and a longer transfer time, $T = 6.36$ days. Certainly, transfers to QPDROs appear to be an interesting alternative.

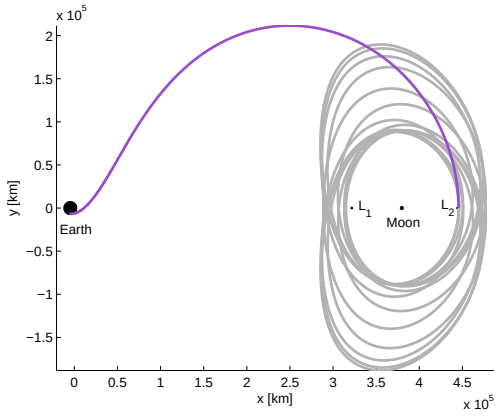

Figure 10. Transfer to QPDRO at $C = 2.91$

Despite constraining the QPDRO energy level to one value and the insertion location to the lunar far-side, transfers to a particular QPDRO still offer an infinite variety of insertion locations, each corresponding to a different x-position and velocity within the stability region. Moreover, an infinite number of QPDROs exist at a particular energy level. Of course, the ΔV cost and TOF vary for transfers to different locations within the stability region at a particular energy level. For example, Figures 11(a)-11(b) highlight the DRO stability region captured at $y = 0$ and $C = 2.91$ and outlined in black by the P3DRO manifolds at this energy level. The DRO at this energy level appears as a black dot at the center of the stability region. Unsurprisingly, given that transfers to QPDROs are similar to Hohmann arcs, the LEO departure cost increases, almost exclusively, with increasing QPDRO insertion location along the x-axis. However, the overall variation in departure cost, $3.1495 \leq \Delta V_1 \leq 3.1547$ km/s, is relatively small; the variation in the insertion maneuver, $579.2455 \leq \Delta V_2 \leq 620.2080$ m/s, is apparent in Figure 11(a). The range in transfer TOF, $5.86 \leq T \leq 7.23$

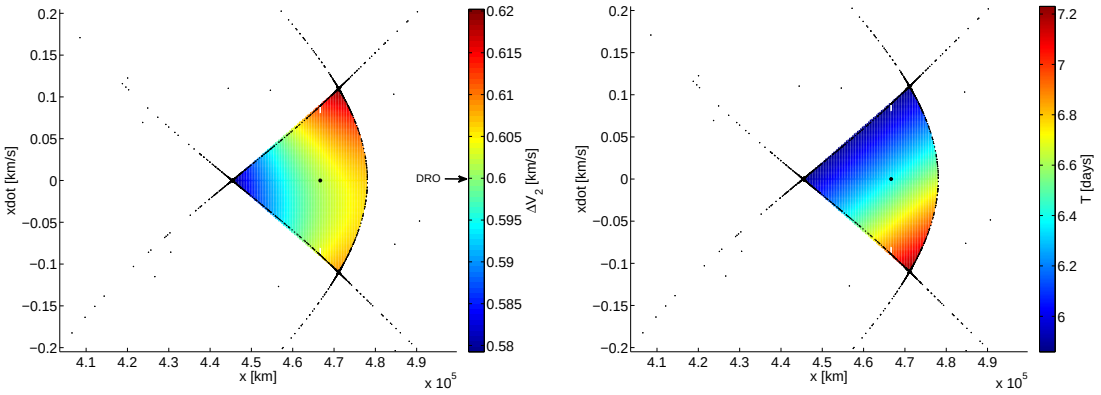

(a) QPDRO insertion cost (b) TOF

Figure 11. Direct Transfers into DRO stability region, $C = 2.91$

days, is easily appreciated from Figure 11(b). Transfers with negative arrival x-velocity "overshoot" the final location to achieve the final condition, and therefore require more time to reach the QPDRO insertion location than transfers with positive arrival x-velocity. Therefore, certain locations within the quasi-periodic region are associated with faster and cheaper transfers to the stability region, than the single DRO at the same energy level. Targeting the stability region in nearly equivalent to targeting the DRO. The QPDRO may offer advantages when transitioning to higher fidelity models.

The DRO stability region can also be employed as an intermediate step to deliver the spacecraft from LEO to a lunar near-side DRO insertion. For example, the transfer to the DRO at $C = 2.91$ in Figure 12 is constructed by combining a transfer to a QPDRO (at a lower Jacobi constant than the destination DRO), a specified number of lunar revolutions along the QPDRO, and a lunar near-side DRO insertion maneuver. For this transfer the total ΔV is marginally less costly than the direct transfer with a lunar far-side DRO

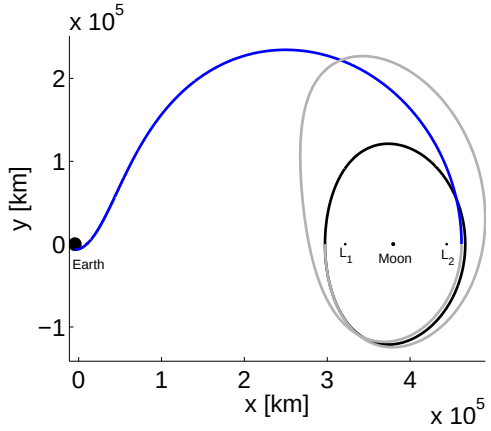

Figure 12. Transfer to DRO via QPDRO

insertion for the same destination DRO. The sample transfer to the QPDRO was constructed to exploit the DRO stability region at different energy levels to reduce the maneuver cost. Therefore, TOF is not particularly meaningful in this type of transfer because the QPDRO insertion location can always be adjusted to meet a specific TOF requirement.

In the presence of perturbations in higher fidelity models, DROs appear as QPDROs. Therefore, trans-

fers to DROs are essentially transfers to QPDROs. Hence, transfers to QPDROs can be very useful when transitioning solutions to a higher-fidelity ephemeris model.

Transfers to Lunar DROs in the Ephemeris Model

To validate the characteristics of the transfer trajectories, sample transfers are transitioned into a higher-fidelity model and, in fact, generally retain their geometry, maneuver costs and TOF. This evaluation is achieved using the ATD software.[23] First, the transfer trajectory, as well as several revolutions of the destination DRO are discretized into numerous arcs, represented as position and velocity states, and saved in a suitable format to interface with ATD. These states are then imported and, within the ATD environment, corrected for continuity in position and velocity (except at maneuver locations) in an ephemeris model. Before the corrections process is applied, however, several options are specified:

1. Ephemeris epoch: The ephemeris date corresponding to the first discretized state must be specified. In this investigation, the first discretized state is located at departure from LEO, and each sample transfer is converged in the ephemeris model for epochs corresponding to the first day of every month in the calendar year 2021. Furthermore, the departure epoch is constrained at the desired date throughout the corrections process.

2. Central and perturbing bodies: The central and perturbing bodies are selected to characterize the equations of motion to propagate the imported states. Here, the Earth is specified as the central body, and the Sun and Moon are included as perturbing bodies.

3. Reference CR3BP: The reference CR3BP system is specified for viewing and output purposes. The Earth-Moon CR3BP is selected in the current analysis.

4. Apse, altitude, and inclination constraints: Specific states may be required to remain at a specified altitude, to occur at an apse corresponding to a specific gravitational body, or to possess some inclination with respect to a specific central body's equator throughout the corrections process. For the transfer paths here, the first state is constrained to be a 200-km altitude perigee, at 28.5° inclination with respect to the Earth's equatorial plane.

5. Maneuver locations: The ATD differential corrections process adjusts the states to produce a path continuous in position and velocity, except at locations where maneuvers are allowed. These maneuver locations are specified before the corrections process is applied. Direct transfers with lunar far-side insertions incorporate one maneuver at the DRO insertion location, while direct transfers via an L_1 Lyapunov orbit with a lunar near-side DRO insertion include one maneuver at the Lyapunov orbit insertion point, and one at the DRO insertion point.

In ATD, all trajectories converged in the ephemeris model are viewed in the reference CR3BP rotating, barycentered frame. Thus, unless otherwise stated, all discussion related to results obtained in the ephemeris model in this investigation are reported with respect to the reference Earth-Moon CR3BP rotating, barycentered frame.

Two transfers to the DRO that exists at $C = 2.91$ in the Earth-Moon CR3BP system are selected for transition to the ephemeris model incorporating the Sun, Earth and Moon gravitational fields. The first path is directly targeted to the lunar far-side of the DRO for insertion, while the second arrives at the near-side of the Moon, initially inserts into an L_1 Lyapunov orbit and, after a half-period along the Lyapunov, it reaches the DRO. Projections onto the xy, xz, yz planes, as well as a three-dimensional view of these transfers are plotted in Figures 13(a) and 13(b), respectively, as they appear (after convergence) in the ephemeris model, and as viewed in the rotating, barycentered Earth-Moon frame for departure epoch January 01, 2021, 0 hours. The "$*$" symbol denotes the maneuver points. For different departure epochs, solutions similar to that for January 01, 2021, 0 hours can also be computed in the ephemeris model. In this investigation, solutions for departure epochs on the first day of every month throughout the calendar year 2021 are calculated. The magnitude of each maneuver, as well as the TOF (first approach to the lunar region) are summarized in Figures 14-15 as a

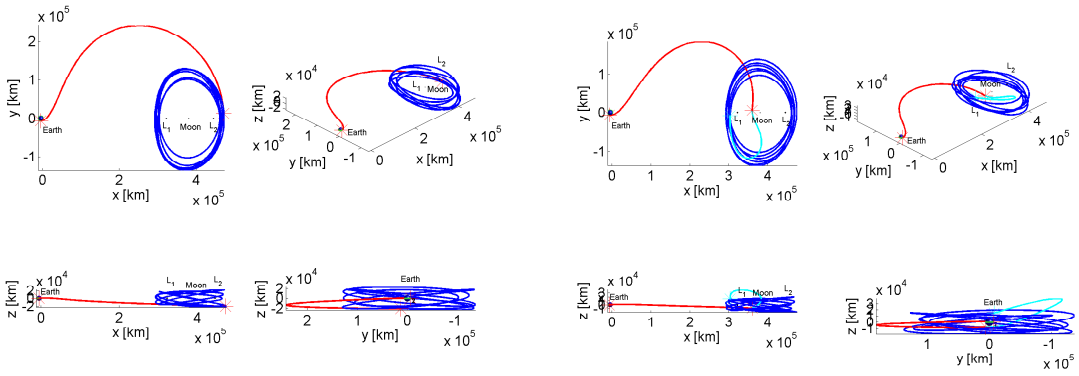

(a) Lunar far-side DRO insertion

(b) Lunar near-side DRO insertion

Figure 13. Transfers to DRO (CR3BP $C = 2.91$) converged in the ephemeris model for departure epoch of January 01, 2021, 0 hours as viewed in the rotating, barycentered Earth-Moon frame.

function of the corresponding ephemeris date. The black circles indicate the value for the quantity associated with the ephemeris model solution, and the flat blue lines highlight the values that characterize the initial guess from the planar CR3BP.

The variations in the results are clearly influenced by the impact of the perturbing bodies on the initial guess as the trajectory is corrected for continuity in the ephemeris model corresponding to different epochs in 2021. As a demonstration of the impact, and for prediction purposes, consider the distance between the Earth and the Moon in 2021 plotted in the top plot in Figure 16, and the inclination of the Moon's orbit with respect to Earth's equatorial plane plotted in the bottom plot of the same figure. The daily values appear in black. The values at each departure date are highlighted in green, while the values at the arrival time in the lunar region are highlighted in red for the far-side insertion case, and in purple for the near-side insertion transfers. For transfers to the near-side, recall that one additional maneuver is required to insert into the DRO. The values corresponding to this maneuver are highlighted in light blue. Clearly, the Earth-to-Moon distance at departure influences the magnitude of the departure maneuver, ΔV_1 (which is also naturally influenced by the solar position). The farther the Earth-to-Moon distance, the larger the departure maneuver is, consistent with any Hohmann transfer. Similarly, the transfer time increases as the distance between the Earth and the Moon at the departure epoch increases. For the transfer to the lunar far-side, the DRO insertion maneuver decreases with increasing distance between the Earth and the Moon at arrival. For different departure epochs in the ephemeris model, the transfer insertion location shifts across the width of the DRO stability region. When the Moon is closest to the Earth, so is the stability region, dictating that the initial guess from the CR3BP is shifted to the outer-most part of the stability region. Therefore, the converged solution yields a transfer path that inserts into the most expensive part of the stability region, as previously noted in Figure 11(a). Conversely, when the Moon is farthest from the Earth, the CR3BP initial guess yields a trajectory in the ephemeris model with an insertion to the inner-most, and less expensive, part of the stability region. Furthermore, the distance and orientation of the Sun with respect to the Earth-Moon system is also influential.

DRO Stationkeeping

Given that a potential application for distant retrograde orbits in the Earth-Moon system is future manned missions to lunar DROs, an assessment of the stationkeeping (SK) costs associated with maintaining such orbits is useful. For this initial consideration of stationkeeping, the investigation refers to the model in the CR3BP. The long-term SK strategy described by Pavlak is employed for a preliminary consideration of DRO maintenance.[24] Such a scheme is particularly useful in dynamically sensitive regimes. Given a trajectory that is continuous in position and velocity in a particular model, this SK scheme uses a multiple-shooting

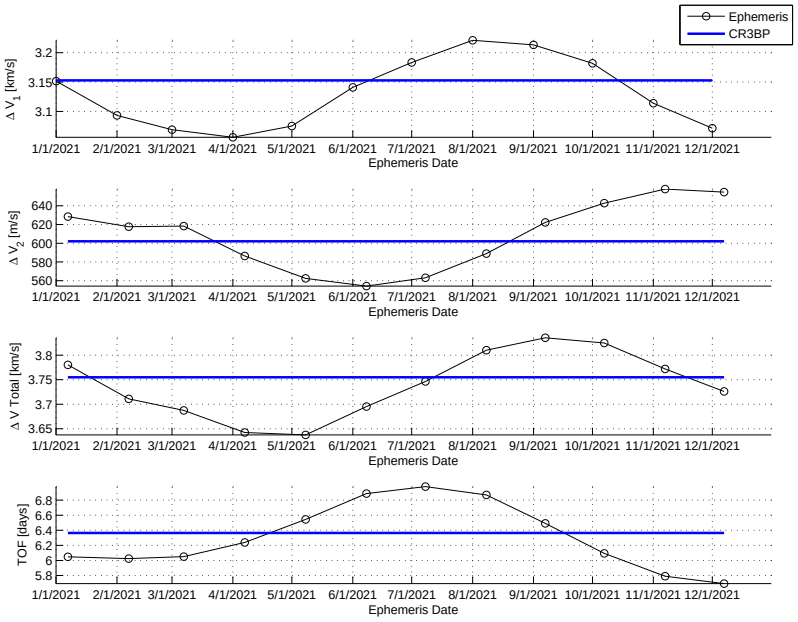

Figure 14. Variation in maneuver size and TOF throughout year 2021 for transfer to DRO (CR3BP $C = 2.91$) with lunar far-side insertion in ephemeris model.

algorithm combined with a sequential quadratic programing direct optimization routine to compute each SK maneuver that is required to maintain the given trajectory in the presence of navigation/modeling and maneuver execution errors. First, the SK keeping costs associated with periodic orbits across the planar DRO family are computed for a baseline error level. The DRO at $C = 2.91$ is a representative orbit for the SK analysis, one that is beyond the Earth-Moon libration points, i.e., beyond the Hill region. Thus, the SK costs are expected to be relatively smooth. Three additional scenarios compare the SK cost associated with the DRO that exists at $C = 2.91$ to:

1. DROs in 1:3 and 2:3 resonance with the Moon
2. A QPDRO at $C = 2.91$
3. An adjacent L_1 Lyapunov orbit

Each scenario considers higher error levels in comparison to the baseline set that is employed across the planar DRO family.

An initial exploration of SK across the family offers context. In the computation of SK costs associated with select members of the planar DRO family, navigation/modeling errors are simulated as random, and normally distributed with 1-σ statistics equal to 1 km in position and 1 cm/s in velocity. Additionally, after each SK maneuver is computed, a 1-σ maneuver execution error of 1% (in magnitude only) is applied. In this analysis, each periodic orbit is maintained over 12 periods, with maneuvers at each crossing of the xz-plane in the rotating frame. The final crossing is constrained to match the original trajectory in the x and z-position. Then, the total SK ΔV cost associated with the maintenance of each orbit is the resulting mean of 500 Monte Carlo trials, extrapolated for 1 year of maintenance operations. When applied to the family of lunar DROs in the Earth-Moon CR3BP model, the costs in Figure 17 are obtained. Recall the range of DRO orbital periods in Figure 1(b). The three DROs plotted in dashed black lines in Figure 17 are periodic orbits in the planar DRO family that bifurcate to other families. The smallest and intermediate amplitude DROs

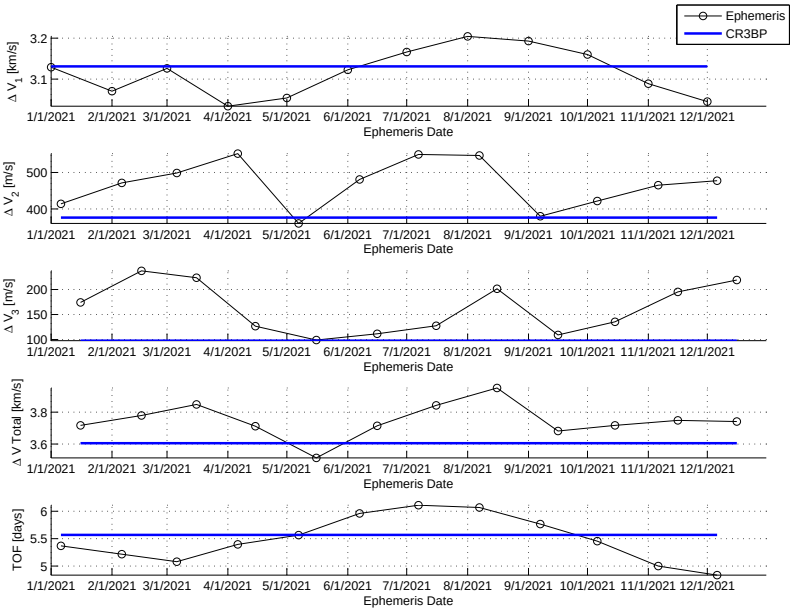

Figure 15. Variation in maneuver size and TOF throughout year 2021 for transfer to DRO (CR3BP $C = 2.91$) with lunar near-side insertion in ephemeris model.

plotted in dashed black lines are in 1:3 and 2:3 resonances with the Moon, respectively, and are bifurcating orbits with the planar family of P3DROs. The largest DRO in dashed black is the out-of-plane bifurcation orbit, a member of both the planar and three-dimensional families of DROs as described by Vaquero and Howell.[14,15] The range for SK costs in these DROs, i.e., 0-14 m/s, total for a one year maintenance strategy, is reasonably low when compared to other orbits in the lunar region. For example, given a comparable error framework, L_1 and L_2 Lyapunov, halo and quasi-halo orbits possess SK costs in an approximate range of 0-35 m/s. Similar to the L_1 and L_2 orbit families, DRO SK costs increase as stability decreases.[24] In particular, there are specific regions where SK costs are noticeably higher than those throughout the rest of the family. These regions coincide with the 1:3, 2:3 and out-of-plane bifurcations. Also, as expected, higher SK costs are associated with unstable DROs than those that are stable.

Given a variety of potential applications for lunar DROs, SK costs are investigated in the presence of larger navigation/modeling and maneuver execution errors. The navigation/modeling errors considered for the first two scenarios are summarized in Table 2. Three examples are explored. In each sample, results for the

Table 2. High error levels

Multiplication Factor	Position Error [km]	Velocity Error [cm/s]
$\times 1$	1	1
$\times 10$	10	10
$\times 100$	100	100

representative DRO are compared to other notable orbits as mentioned previously. In the first scenario, the SK costs for a DRO with a 16.4421-day orbital period ($C = 2.91$) is compared to each of the planar DROs in resonance with the Moon. The SK costs are computed for the three error levels as described in Table 2. The results, summarized in Figure 18, reveal that for "$\times 1$" and "$\times 10$" error levels, the orbits in resonance with

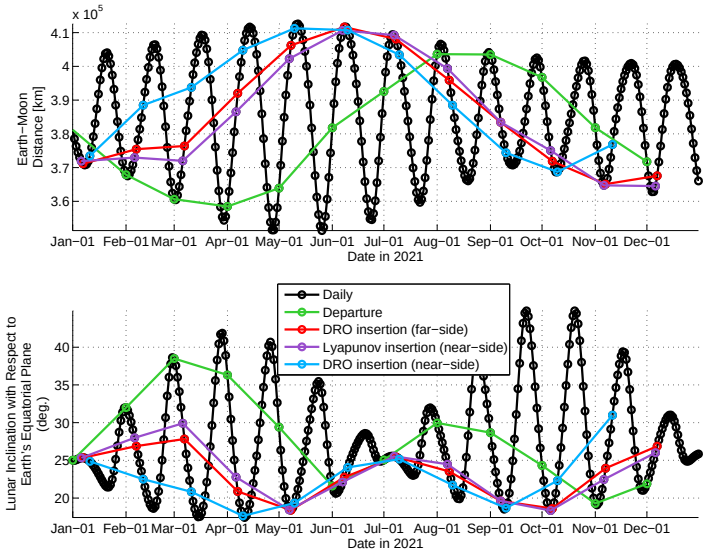

Figure 16. Distance between the Earth and the Moon (top plot), and lunar inclination with respect to the Earth's equatorial plane (bottom plot) throughout year 2021

the Moon require higher SK costs for maintenance, than the non-resonant orbit. However, at the highest error level "$\times 100$", perhaps exceeding the linear range, the SK costs are more competitive.

The second scenario compares SK costs for the same representative DRO as emphasized in scenario 1, and the QPDRO plotted in black in Figure 19(a) at the same energy level, $C = 2.91$. For each Monte Carlo simulation, the final QPDRO crossing of the x-axis is constrained to remain within $\pm 2,500$ km in the x and z directions relative to the initial state. The resulting QPDRO, including the maintenance maneuvers, is plotted in blue in Figure 19(a), and the red "$*$" symbol denotes the SK maneuver locations. It is apparent, and not surprising, that the QPDRO shifts to the boundary of the constraints in x as the corrections and optimization process is applied. The SK costs for both orbits are summarized in Figure 19(b). Clearly, a lower SK cost is associated with maintaining the QPDRO rather than the DRO at all three error levels considered in this investigation. For the QPDRO, the looser constraints on the x-axis crossing is beneficial. However, more investigation is required for the Monte Carlo simulations since $\leq 10\%$ of the trials did not converge for the higher error level "$\times 100$".

The third scenario compares SK costs for the DRO and Lyapunov orbit in Figure 5(b). Due to the close lunar passage present in the rather large Lyapunov orbit, this motion is difficult to maintain. Moreover, a significant % of the Monte Carlo simulations may not converge if numerous Lyapunov revolutions are required, and/or a high maneuver execution % error is applied. Therefore, to obtain ≥ 99.99 % converged trials, only 3 Lyapunov revolutions are required, and only 1% of the maneuver magnitude execution error is applied. However, the DRO is still maintained for 12 revolutions, and a 2% maneuver execution error is applied. The resulting SK costs for the DRO and Lyapunov orbit are compared in Figure 20. Although this scenario considers significantly smaller error levels, it is evident that the Lyapunov orbit requires SK costs that increase at a higher rate than that required to maintain the DRO. However, recall that this representative DRO remains beyond the Hill region. The relatively large Lyapunov orbit does enter the region between the Moon and L_1; the perturbations are significantly influenced by the relatively close lunar pass.

CONCLUDING REMARKS

Through this investigation, DRO characteristics such as stability, period, and properties of the surrounding stability region were found insightful in the analysis of SK costs associated with maintaining motion along a

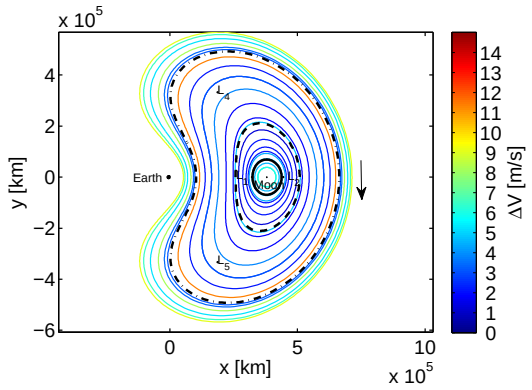

Figure 17. Earth-Moon SK costs in CR3BP across the DRO family

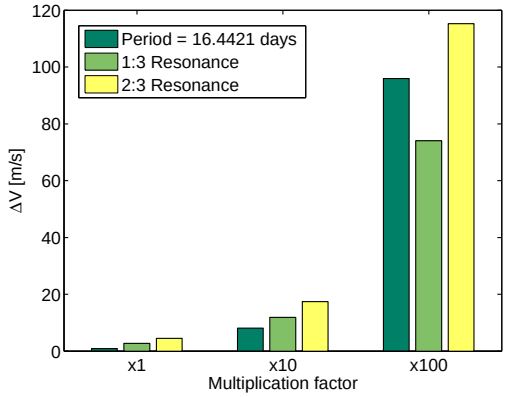

Figure 18. Scenario 1: DRO SK in CR3BP in the presence of high error levels

DRO, and the behavior in the ephemeris model. The different transfer strategies explored provide a baseline understanding of the costs and TOFs associated with the dynamics of traveling to DROs and the surrounding stability region from Earth. Several transfer options were indentified, including direct transfers with lunar near- and far-side DRO insertion, as well as transfers into QPDROs. In particular, transfers into QPDROs facilitate the understanding of solution characteristics when transitioned to an ephemeris model. This investigation also revealed relatively low SK costs associated with DROs, with isolated exceptions that can be predicted from the stability information available for DROs from the CR3BP analysis. These preliminary results suggest future directions for additional work. Such investigations are ongoing.

ACKNOWLEDGMENTS

The authors appreciate the support from the Purdue University School of Engineering Education. Also many thanks to Amanda Haapala, and Dr. Thomas Pavlak for their assistance with the computations. Portions of the work were also completed under NASA Grant Nos. NNX13AE55G and NNX13AH02G.

REFERENCES

[1] B. Muirhead, "Asteroid Redirect Robotic Mission (ARRM) Reference Mission Concept Study Public Information Package V1," Aug. 2013. NASA, JPL. [Retrieved Nov. 26,

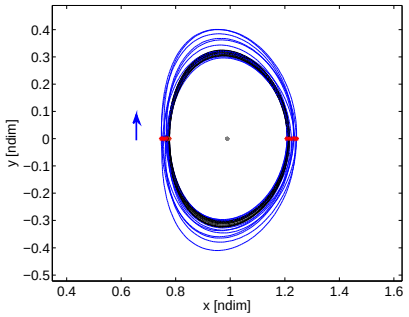

(a) Reference QPDRO and maintained trajectory

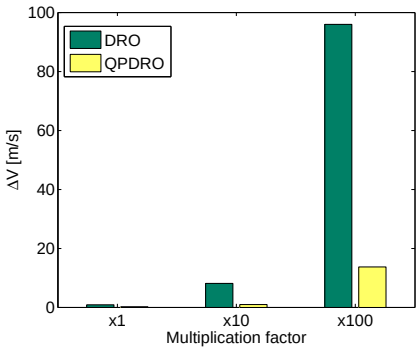

(b) DRO vs. QPDRO SK in CR3BP in the presence of high error levels

Figure 19. Scenario 2: DRO vs. QPDRO, both at $C = 2.91$

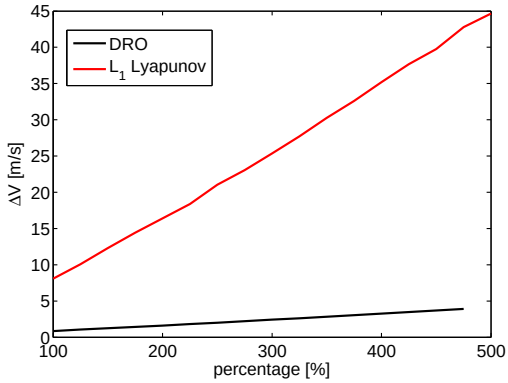

Figure 20. Scenario 3: DRO vs. L_1 Lyapunov SK in CR3BP under high error levels

2013] http://www.nasa.gov/sites/default/files/files/Asteroid-Redirect-Robotic-Mission-Muirhead-TAGGED2.pdf.

[2] S. Stich, "Asteroid Redirect Mission Crewed Mission (ARCM) Concept Study," 2013. NASA, JSC. [Retrieved Nov. 26, 2013] http://www.nasa.gov/sites/default/files/files/Asteroid-Crewed-Mission-Stich-TAGGED2.pdf.

[3] M. Hénon, "Numerical Exploration of the Restricted Problem. V. Hill's Case: Periodic Orbits and Their Stability," *Astronomy and Astrophysics*, Vol. 1, 1969, pp. 223–238.

[4] M. Hénon, "Numerical Exploration of the Restricted Problem. VI. Hill's case: Non-Periodic Orbits," *Astronomy and Astrophysics*, Vol. 9, 1970, pp. 24–36.

[5] V. Markellos, "Numerical Investigation of the Planar Restricted Three-Body Problem. II. Regions of Stability for Retrograde Satellites of Jupiter as Determined by Periodic Orbits of the Second Generation," *Celestial Mechanics*, Vol. 10, 1974, pp. 87–134.

[6] O. C. Winter, "The Stability Evolution of a Family of Simply Periodic Lunar Orbits," *Planetary and Space Science*, Vol. 48, No. 1, 2000, pp. 23–28.

[7] C. Douskos, V. Kalantonis, and P. Markellos, "Effects of Resonances on the Stability of Retrograde Satellites," *Astrophysics and Space Science*, Vol. 310, No. 3-4, 2007, pp. 245–249.

[8] C. A. Ocampo and G. W. Rosborough, "Transfer Trajectories for Distant Retrograde Orbiters of the Earth," *AAS*, No. 93-180, 1993, pp. 1177–1200.

[9] T. Lam and G. J. Whiffen, "Exploration of Distant Retrograde Orbits Around Europa," *15th AAS/AIAA Space Flight Mechanics Conference*, Copper Mountain, Colorado, 2005.

[10] J. Demeyer and P. Gurfil, "Transfer to Distant Retrograde Orbits Using Manifold Theory," *Journal of Guidance, Control and Dynamics*, Vol. 30, No. 5, 2007, pp. 1261–1267.

[11] C. J. Scott and D. B. Spencer, "Stability Mapping of Distant Retrograde Orbits and Transport in the Circular Restricted Three-Body Problem," *AIAA/AAS Astrodynamics Specialist Conference and Exhibit, 18 - 21 August*, Honolulu, Hawaii, 2008.

[12] C. J. Scott and D. B. Spencer, "Calculating Transfer Families to Periodic Distant Retrograde Orbits Using Differential Correction," *Journal of Guidance, Control and Dynamics*, Vol. 33, No. 5, 2010, pp. 1592–1605.

[13] X. Ming and S. Ming, "Exploration of Distant Retrograde Orbits Around Moon," *Acta Astronautica*, Vol. 65, 2009, pp. 853–860.

[14] M. Vaquero and K. C. Howell, "Leveraging Resonant Orbit Manifolds to Design Transfers between Libration Point Orbits in Multi-Body Regimes," *23rd AAS/AIAA Space Flight Mechanics Meeting*, No. AAS 13-334, Kauai, Hawaii, February 2013.

[15] M. Vaquero and K. C. Howell, "Leveraging Resonant-Orbit Manifolds to Design Transfers Between Libration-Point Orbits," *Journal of Guidance, Control, and Dynamics*, 2014, DOI: 10.2514/1.62230.

[16] V. Szebehely, *Theory of Orbits: The Restricted Problem of Three Bodies*. New York: Academic Press Inc., 1967.

[17] R. A. Broucke, "Periodic Orbits in the Restricted Three-Body Problem with Earth-Moon Masses," Tech. Rep. 32-1168, Jet Propulsion Laboratory, 1968.

[18] J. S. Parker and G. H. Born, "Direct lunar halo orbit transfers," *The Journal of the Astronautical Sciences*, Vol. 56, No. 4, 2008, pp. 441–476.

[19] R. R. Rausch, "Earth to Halo Orbit Transfer Trajectories," M.S. Thesis, School of Aeronautics and Astronautics, Purdue University, West Lafayette, IN, August 2005.

[20] D. C. Folta, T. A. Pavlak, A. F. Haapala, and K. C. Howell, "Preliminary Design Considerations for Access and Operations in Earth-Moon L1/L2 Orbits," *23rd AAS/AIAA Space Flight Mechanics Meeting*, No. AAS 13-339, Kauai, Hawaii, February 2013.

[21] A. E. Roy and M. W. Ovenden, "On the Occurrence of Commensurable Mean Motions in the Solar System. The Mirror Theorem," *Monthly Notices of the Royal Astronomical Society*, Vol. 115, 1955, pp. 296–309.

[22] D. P. Gordon, "Transfers to Earth-Moon L_2 Halo Orbits Using Lunar Proximity and Invariant Manifolds," M.S. Thesis, School of Aeronautics and Astronautics, Purdue University, West Lafayette, IN, August 2008.

[23] A. F. Haapala, M. Vaquero, T. A. Pavlak, K. C. Howell, and D. C. Folta, "Trajectory Selection Strategy for Tours in the Earth-Moon System," *AAS/AIAA Spaceflight Mechanics Meeting*, No. AAS 13-782, Hilton-Head, South Carolina, August 2013.

[24] T. A. Pavlak, "Trajectory Design and Orbit Maintenance Strategies in Multi-Body Dynamical Regimes," Ph.D. Dissertation, School of Aeronautics and Astronautics, Purdue University, West Lafayette, IN, May 2013.